Pseudo-direct to direct compositional crossover in wurtzite GaP/InxGa1-xP core-shell nanowires

Journal:	*Nano Letters*
Manuscript ID	nl-2016-04242a.R1
Manuscript Type:	Communication
Date Submitted by the Author:	16-Nov-2016

Complete List of Authors:	Gagliano, Luca; Technische Universiteit Eindhoven, Applied Physics Belabbes, Abderrezak; King Abdullah University of Science and Technology Albani, Marco; Università degli Studi di Milano-Bicoccaàààààà, Dipartimento di Scienza dei Materiali Assali, Simone; TU/e, Applied Physics Verheijen, Marcel; Technische Universiteit Eindhoven, Philips Innovation Labs Miglio, Leo; Università degli Studi di Milano-Bicoccaàààààà, Dipartimento di Scienza dei Materiali Bechstedt, Friedhelm; Friedrich-Schiller-Universitaet Jena, Institut fuer Festkoerpertheorie und -optik Haverkort, Jos; TU/e, Applied Physics Bakkers, Erik; Delft University, Kavli Institute

Pseudo-direct to direct compositional crossover in wurtzite GaP/$In_xGa_{1-x}P$ core-shell nanowires

L. Gagliano[1,*], A. Belabbes[2,3], M. Albani[4], S. Assali[1], M. A. Verheijen[1,5], L. Miglio[4], F. Bechstedt[3], J.E.M. Haverkort[1], E.P.A.M. Bakkers[1,6]

[1] *Dept. of Applied Physics, Eindhoven University of Technology, 5600 MB Eindhoven, The Netherlands*
[2] *King Abdullah University of Science and Technology (KAUST), Physical Science and Engineering Division (PSE) Thuwal 23955-6900, Saudi Arabia*
[3] *Institut für Festkörpertheorie und -optik, Friedrich-Schiller-Universitat, Max-Wien-Platz 1, D-07743 Jena, Germany*
[4] *L-NESS and Dept. of Materials Science, University of Milano Bicocca, 20125, Milano, Italy*
[5] *Philips Innovation Labs Eindhoven, High Tech Campus 11, 5656AE Eindhoven, The Netherlands*
[6] *Kavli Institute of Nanoscience, Delft University of Technology, 2600 GA Delft, The Netherlands*

* l.gagliano@tue.nl

Thanks to their uniqueness, nanowires allow the realization of novel semiconductor crystal structures with yet unexplored properties, which can be key to overcome current technological limits. Here we develop the growth of wurtzite GaP/$In_xGa_{1-x}P$ core-shell nanowires with tunable Indium concentration and optical emission in the visible region from 590nm (2.1eV) to 760nm (1.6eV). We demonstrate a pseudo-direct (Γ_{8c}-Γ_{9v}) to direct (Γ_{7c}-Γ_{9v}) transition crossover through experimental and theoretical approach. Time resolved and temperature dependent photoluminescence measurements were used, which led to the observation of a steep change in carrier lifetime and temperature dependence by respectively one and three orders of magnitude in the range $0.28\pm0.04\leq x\leq0.41\pm0.04$. Our work reveals the electronic properties of wurtzite $In_xGa_{1-x}P$.

KEYWORDS: semiconductor nanowire, indium gallium phosphide, wurtzite, band crossover, heterostructure

A new degree of freedom in band structure engineering has become available in the form of crystal phase tuning in semiconductor nanowires, allowing the control of the material polytype[1–4]. Crystal phase engineering thus unlocks new optical and electronic properties while maintaining compatibility with well-established mainstream semiconductor technology. This provides a promising method to surpass the conventional limits of commonly used semiconductors[5–9]. Various nanowire growth mechanisms[2,4,10,11] enable the formation of unusual crystal phases which are not accessible in bulk[2,4,12–16], such as Wurtzite (WZ) in III-Phosphides, and by exploiting 3D epitaxial overgrowth such crystal phase can be transferred from the core to its surrounding shell[17].

Wurtzite nanowires are very promising candidates for solid state lighting[4,14–16], photovoltaics[18] and solar hydrogen conversion[19,20]. Recently it has also been shown that Wurtzite III-Phosphides enable direct band gap green emitters, opening a promising way to "bridge the green gap"[21]. WZ GaP and WZ InP have been studied, both theoretically[22–24] and experimentally, and their optical properties are known[4,15,25,26]. Both materials have a Γ_{9v} highest valence band but, importantly, the first two conduction bands have a different order: the lowest conduction band in WZ GaP has Γ_{8c} symmetry, followed by a Γ_{7c} band at higher energy[24,27]. In WZ InP this situation is reversed and Γ_{7C} is the lowest band. This has a strong influence on the optical properties of the materials as the Γ_{8C} - Γ_{9V} transition is allowed with a weak oscillator strength, while the Γ_{7C} - Γ_{9V} is instead allowed with a large oscillator strength, as in WZ GaAs and WZ InP[28]. By tuning the $In_xGa_{1-x}P$ composition a crossover at the Γ point is expected, where the Γ_{8c} (lowest for Ga-rich) will be crossed by the Γ_{7c} band for increasing In concentrations. Such a Γ-crossing has not been observed so far

for III-V semiconductors through compositional tuning. Moreover, the electronic properties of the WZ $In_xGa_{1-x}P$ alloy are still fully unexplored.

In this work we achieve the growth of WZ $In_xGa_{1-x}P$ alloys through crystal structure transfer[17] in WZ GaP/$In_xGa_{1-x}P$ core-shell nanowires and study their optical properties. We demonstrate emission tunability between 590nm (2.1eV) and 760nm (1.6eV). The decrease by one order of magnitude in the lifetime of the optically generated carriers combined with the strong increase in optical emission for Indium contents higher than x≥0.4 demonstrates the pseudo-direct to direct Γ_{8C} - Γ_{7C} crossover. The large oscillator strength of the Γ_{7C} - Γ_{9V} transition makes WZ $In_xGa_{1-x}P$ suitable for solid-state emitters in the red and infrared range, while still having a relevant application for solar hydrogen conversion due to its wide and tunable band gap.

WZ GaP/$In_xGa_{1-x}P$ core-shell nanowires are grown by a multi-step method, featuring WZ GaP core vapor-liquid-solid (VLS) growth[4] (schematic layout in Fig. 1a). The Au catalyst droplets for VLS growth were fabricated using nanoimprint lithography on a square matrix with a 500nm pitch or on a hexagonal matrix with 2500nm pitch. The low defectivity (<1 stacking fault/μm) WZ GaP cores were then grown with Metalorganic Vapor Phase Epitaxy (MOVPE) at 615˚C, using Trimethylgallium (TMGa) and Phosphine (PH_3) as precursors, in combination with Hydrogen Chloride (HCl) to suppress sidewall tapering[4]. The Au catalyst was subsequently removed from the nanowire top to suppress further axial growth with an *ex-situ* wet etching, using King's Water and Iodine solution with optimized concentration and etching times (see Supporting Information S1). The etched cores were then used as a template for the shell growth at 585˚C in the same reactor, using Trimethylindium (TMIn) as Indium

precursor with a very high V/III ratio (>1000 in our case) in order to promote layer growth[29].

Hydrogen Chloride (HCl) is also used to control the morphology of the layer growth[30] (see Supporting Information S2 for details).. HCl has two important effects on the shell growth[2,4,31–35]. Firstly, it etches material from the nanowire surfaces, preferentially etching Indium over Gallium[36]. This effect can also be used as an additional degree of freedom to control the effective Indium incorporation during the layer growth. Secondly, HCl passivates the surface of III-Phosphides, leading to a progressive saturation of the surface by Chlorine, eventually stopping the growth and limiting the maximum thickness of the shell to about 20-40 nm. This surface passivation effect can be avoided by applying a growth process featuring two alternating steps: a 15 minutes long growth step as we described earlier, alternated by a 45s step to remove the passivation layer. The passivation removal step is performed with a lower HCl flow and a higher Gallium flow, providing no Indium. During this step, TMGa reacts with Chlorine at the nanowire sidewalls, producing $GaCl_3$ and thereby removing the passivation layer[13]. Using this cyclic growth, an arbitrarily thick WZ InGaP shell can be grown.

The resulting structures have been characterized by Scanning Electron Microscopy (SEM). The WZ GaP/$In_{0.24}Ga_{0.76}P$ wires in Fig. 1b are uniform and may bend in random directions with an angle up to 10 degrees. $In_xGa_{1-x}P$ in fact possesses a larger lattice parameter than GaP and we expect the shell to be compressively strained. Bending is due to possible asymmetrical defect density and/or composition in the shell[37] and this feature will be investigated more in detail in a forthcoming work.

The morphology and the crystal quality, *i.e.* the purity of the WZ phase and the absence of defects are analyzed with Transmission Electron Microscopy (TEM). For this study the overall structures need to be sufficiently transparent to the electron beam in order to allow high-resolution imaging and therefore a maximum diameter of about 140 nm is used with a 15nm shell thickness. As shown in Fig. 2a, the $In_xGa_{1-x}P$ shell shows a WZ crystal structure. Shells with low Indium content (up to x=0.10) are defect-free (as shown in Supporting Figure S2), while the wires with higher Indium content show misfit dislocations (arrow in Fig. 2a). The shell composition is determined by Energy-dispersive X-Ray Spectroscopy (EDS), as shown in Figures 2b-d. We used the EDS data to calibrate the precursor flows to obtain the desired average composition of each shell. The experiment is performed in two different crystallographic orientations: in projection (Fig. 2b) along the $[11\bar{2}0]$ zone axis, and in cross-section (Fig. 2c-e), with the nanowire cut perpendicularly to its main $[0001]$ axis. Cross-sectional analysis is necessary to observe the surface faceting and to observe the inner structure of the shell. From the cross-sectional EDS analysis shown in Fig. 2c-e we obtain an average Indium fraction of x=0.24±0.04 for this sample. Regions with lower Indium concentration are visible along the rods radially extending from the corners of the hexagonal core (see Supporting Information S3), a phenomenon also observed in previous work on core-shell nanowires[7,38,39]. A 2-5nm thin shell with lower Indium concentration (~5-10%) can also be observed in fig. 2d in between two WZ InGaP shells with higher Indium content, resulting from the layer growth during the chlorine removal step after growing the first $In_xGa_{1-x}P$ shell. The facets of the WZ $In_xGa_{1-x}P$ shells belong to two different families: $\{1\bar{1}00\}$ parallel to the core facets and $\{11\bar{2}0\}$. The number of facets increases with shell thickness as it is possible that the $\{11\bar{2}0\}$ facets

in WZ $In_xGa_{1-x}P$ are low energy facets which appear to minimize the total surface energy. Also, the substitution of the corner between $\{1\bar{1}00\}$ facets with a $\{11\bar{2}0\}$ facet likely helps to minimize the energy.

In order to evaluate the strain magnitude and distribution within the core/shell system, Finite Element Method (FEM) simulations[40] of hydrostatic strain have been performed for a WZ GaP/$In_xGa_{1-x}P$ core-shell nanowire geometry with a core apothem and shell thickness both of 50nm and for a corresponding planar geometry. The results are displayed in Fig. 2f for x=0.25 and x=0.75 (see Supporting Information S4 for x=0.50, x=1 and for more details). A six-fold symmetry is clearly present, with six pockets at lower strain in the shell caused by the geometric relaxation induced by the six corners, in agreement with previous studies[41]. This phenomenon results in a much lower average hydrostatic strain (less than one third) than expected for a corresponding planar $\{1\bar{1}00\}$ heterostructure with identical lattice mismatch as reported in Table 1. This means that the nanowire geometry allows for very efficient strain relaxation, probably delaying the onset of plastic relaxation to shell thickness three times larger than the critical thickness in the planar film (which is not present in the WZ structure) The precise details of the strain relaxation mechanism will be discussed in a future work. For the present report, it is important to mention that these strain effects have been taken into account for the analysis of the photoluminescence results on these structures.

The optical properties of the WZ GaP/$In_xGa_{1-x}P$ core-shell nanowires are investigated by photoluminescence (PL) measurements as a function of the Indium concentration (see Supporting Information S5 for methods). In order to directly correlate the emitted PL wavelength with Indium composition, nanowires are

transferred onto a TEM grid where first PL experiments and then EDS (in TEM) studies are performed on the same nanowires (see Supporting Information S6). With this method we can avoid difficulties arising from wire-to-wire variations. Overall, the emission wavelength shifts from 590nm to 760nm by increasing x from x=0 to x=0.75 (in $In_xGa_{1-x}P$) as shown in Fig. 3a. The emission of all WZ $In_xGa_{1-x}P$ shell compositions is polarized perpendicular to the growth c-axis as shown in Fig. 3b (here a WZ GaP/$In_{0.63}Ga_{0.37}P$ nanowire with degree of polarization 55%), reaching up to 80% polarization in some nanowires, confirming that the emission originates from the WZ crystal structure (also see Supporting Information S5). However, as both the Γ_{8C} and Γ_{7C} conduction bands of WZ $In_xGa_{1-x}P$ are expected[22–24,26] to emit with polarization perpendicular to the nanowire, the polarization selection rules do not allow to discriminate between these two bands.

To identify the bands involved in the emission and to find the Γ_{8C}/Γ_{7C} crossover point as a function of the Indium composition, time-resolved PL (TRPL) measurements are performed at 10K. Two representative TRPL measurements are shown in Fig. 3c from samples with x=0.24±0.04 and x=0.75±0.04 (WZ $In_xGa_{1-x}P$) with lifetimes of 6.2ns and 0.42ns, respectively. Measurements performed over a wide compositional range, averaged on several single nanowires, at 10K show that the emission from WZ $In_xGa_{1-x}P$ shells with $x \leq 0.28 \pm 0.04$ feature lifetimes well above 1ns, while shells with $x \geq 0.45 \pm 0.04$ feature lifetimes well below 1ns, as reported in Fig. 3d, constituting a significant and reproducible difference in lifetime. Since we expect to observe two different predominant recombination mechanisms, Donor Acceptor Pair (DAP) when Γ_{8C} is the lowest conduction band[27], band to band when Γ_{7C} is lowest[15], this difference in lifetime provides a first signature of the Γ_{8C} / Γ_{7C} crossover.

However, such evidence is not conclusive, as the decrease in lifetime could also be attributed to other decay mechanisms, for instance induced by defects in the shell. Temperature-dependent PL measurements were therefore conducted to produce more evidence of the Γ_{8C} / Γ_{7C} crossover. The integrated PL emission intensities as a function of temperature for WZ GaP/$In_{0.24}Ga_{0.76}P$ and WZ GaP/$In_{0.63}Ga_{0.37}P$ are shown in Fig. 4a. The ratio between the integrated emission at 300K (I_{300K}) and 10K (I_{10K}) differs by more than two orders of magnitude between the two samples. We also note that for x≥0.41±0.04 we measured only one single nanowire, while for x≤0.28±0.04 the measurements were performed on an ensemble (5-10) of as-grown wires, since the intensity of the signal at 300K was not sufficient to be detected on single wires: in the inset of Fig. 4a the spectra at 300K of a single WZ GaP/$In_{0.63}Ga_{0.37}P$ core-shell nanowire and of an ensemble of WZ GaP/$In_{0.24}Ga_{0.76}P$ nanowires show the large difference in absolute intensity (~50 times). The values for the I_{300K}/I_{10K} ratio as a function of the Indium content are shown in Fig 4b. Below x=0.28±0.04 values of about 10^{-4} are obtained, while above x=0.41±0.04 the ratio steeply rises by three orders of magnitude, reaching a maximum of 0.18. Since we measure ensembles of wires for x≤0.28±0.04 and single wires for x≥0.41±0.04 we underestimate the variation in I_{300K}/I_{10K}, as the volume of material probed was considerably larger for x≤0.28±0.04. We note therefore that not only the temperature behavior is different, but also the absolute value of I_{300K} is higher by at least two orders of magnitude for x≥0.41±0.04 compared to x≤0.28±0.04, indicating a large difference in oscillator strength.

This steep increase in I_{300K}/I_{10K} ratio in the range 0.28±0.04≤x≤0.41±0.04 is due to the different recombination mechanisms taking place: DAP for x≤0.28±0.04 and band to band for x≥0.41±0.04. This increase is directly correlated with the large

decrease of the PL lifetime shown in Fig. 3, which cannot be explained by the emergence of non-radiative recombination channels, since such channels would result in a lower I_{300K}/I_{10K} ratio[42,43]. On the other hand, this increase in I_{300K}/I_{10K} cannot be explained by a possible passivation effect and suppression of surface recombination due to, for instance, a different surface reconstruction, as this would increase the lifetime[44]. As a conclusion, these experimental data establish the Γ_{8C} / Γ_{7C} crossover for WZ $In_xGa_{1-x}P$ in the compositional range $0.28\pm0.04 \leq x \leq 0.41\pm0.04$.

In order to provide a deeper understanding of the observed transitions, we plot the obtained emission wavelengths as a function of the WZ $In_xGa_{1-x}P$ composition in Fig 4c, obtained by correlation of PL measurements and EDS analysis on the same wires (see Supporting Information S6 for details). In addition, we plot the energy values for the Γ_{7C} - Γ_{9V} transition in WZ GaP and Γ_{8C} - Γ_{9V}, Γ_{7C} - Γ_{9V} transitions in WZ InP available in literature (triangles in Fig. 4c)[23,24,27,45]. As the emission in WZ GaP is impurity-related[27], we report both the emission in this work and the band position from literature. In addition, the band structure of WZ $In_xGa_{1-x}P$ is calculated for different compositions. The calculations have been performed using total-energy calculations in the framework of the density functional theory with the exchange-correlation functional in local density approximation (LDA)[46] as implemented in the Vienna ab initio simulation package (VASP)[47] (see Supporting Information S7). Quasiparticle corrections to account for the excitation aspect are considered in the framework of the LDA-1/2 method[24]. The results are shown in Fig. 4c together with the parabolic fit of the optical transition energies (solid and dotted lines), to facilitate the comparison with the experimental data. The band alignment has also been calculated and found to be Type I for all compositions considered ($x<0.75$, see Supporting

Information S7). Although we note a discrepancy between experimental and calculated data, the results validate our assignment of the PL emission to the Γ_{8C} - Γ_{9V} transition for Indium-poor WZ $In_xGa_{1-x}P$ and to the Γ_{7C} - Γ_{9V} transition for Indium-rich WZ $In_xGa_{1-x}P$. This discrepancy is reasonable, considering the predictive power of the quasiparticle calculations within an accuracy of ±0.1eV. In addition, we should consider alloy disorder and carrier localization effects during the PL measurements, which will result in a lower emission energy, contributing to this discrepancy. From these calculations it is clear that the M minimum cannot be responsible for any observed emission as it is considerably higher in energy.

From the correlation of the PL data with the band structure calculations we can also assess if strain in the shell is a dominant factor. In Fig. 4c we also show (green and red dotted lines) the calculated effect of the average compressive hydrostatic strain on the Γ_{8C} - Γ_{9V} and Γ_{7C} - Γ_{9V} transitions, using the theoretically expected strain without relaxation via defects (Table 1). It can be seen that the band shift compatible with the maximum compressive hydrostatic strain (absence of plastic relaxation) moves the Γ_{8C} - Γ_{7C} crossover towards the WZ InP side. From this it can be concluded therefore that the strain in the nanowires is almost completely relaxed through the previously described geometrical effect and plastic relaxation confirming the structural analysis. The spread obtained in the datapoints in Fig 4c is likely due to a small (≤1%) residual compressive strain in some nanowires, which raises the Γ_{7C} - Γ_{9V} transition to higher energies.

In summary, we demonstrated the growth of WZ GaP/$In_xGa_{1-x}P$ core-shell nanowires with tunable Indium composition of $0 \leq x \leq 0.75 \pm 0.04$, emitting in the visible range between 590nm (2.1eV) and 750nm (1.6eV). We correlated the shortening of

the emission lifetime by one order of magnitude for 0.28±0.04≤x≤0.41±0.04, with a steep rise in I_{300K}/I_{10K} ratio of three orders of magnitude from 10^{-4} to 0.18 in the same composition range. We assigned this difference to the crossover from (pseudo-direct) Γ_{8C} - Γ_{9V} to (direct) Γ_{7C} - Γ_{9V} type of emission as a function of composition and compared these results with theoretical simulations, and find a good qualitative agreement. This work opens the way for the realization of WZ GaP/$In_xGa_{1-x}P$ core-shell nanowire devices, for which we envision applications in solid state lighting, tandem solar cells and solar hydrogen production.

Supporting information

The Supporting Information is available free of charge on the ACS Publications website at XXXXXXXX. Additional information on growth, structure, analysis methods and simulations are provided.

Acknowledgments

We thank S.E.T. ter Huurne and Y.L.W. van Hees for assisting with the measurements, Dr. S. Koelling for the fabrication of the lamellae. This research is jointly supported by the Dutch Technology Foundation STW and Philips Electronics. STW is part of the Netherlands Organization for Scientific Research (NWO), which is partly founded by the Ministry of Economic Affairs. Solliance is acknowledged for funding the TEM facility.

1. Glas, F., Harmand, J.-C. & Patriarche, G. Why Does Wurtzite Form in Nanowires of III-V Zinc Blende Semiconductors? *Phys. Rev. Lett.* **99,** 146101 (2007).

2. Assali, S. *et al.* Exploring Crystal Phase Switching in GaP Nanowires. *Nano Lett.* **15,** 8062–8069 (2015).

3. Jacobsson, D., Lehmann, S. & Dick, K. A. Crystal structure tuning in GaAs nanowires using HCl. *Nanoscale* **6,** 8257–64 (2014).

4. Assali, S. *et al.* Direct band gap wurtzite gallium phosphide nanowires. *Nano Lett.* **13,** 1559–63 (2013).

5. Stark, C. J. M. *et al.* Green cubic GaInN/GaN light-emitting diode on microstructured silicon (100). *Appl. Phys. Lett.* **103,** (2013).

6. Orozco Hinostroza, I. E. *et al.* Tuning emission in violet, blue, green and red in cubic GaN/InGaN/GaN quantum wells. *J. Cryst. Growth* **435,** 110–113 (2016).

7. Berg, A. *et al.* Radial Nanowire Light-Emitting Diodes in the (Al x Ga 1– x) y In 1– y P Material System. *Nano Lett.* **ASAP,** acs.nanolett.5b04401 (2015).

8. Christian, T. M. *et al.* Amber-green light-emitting diodes using order-disorder AlxIn1−xP heterostructures. *J. Appl. Phys.* **114,** 74505 (2013).

9. Oliveira, D. S. *et al.* Interaction between lamellar twinning and catalyst dynamics in spontaneous core–shell InGaP nanowires. *Nanoscale* **7,** 12722–12727 (2015).

10. Jacobsson, D. *et al.* Interface dynamics and crystal phase switching in GaAs nanowires. *Nature* **531,** accepted (2016).

11. Gao, Q. *et al.* Selective-area epitaxy of pure wurtzite InP nanowires: High quantum efficiency and room-temperature lasing. *Nano Lett.* **14,** 5206–5211 (2014).

12. Akopian, N., Patriarche, G., Liu, L., Harmand, J.-C. & Zwiller, V. Crystal phase

quantum dots. *Nano Lett.* **10,** 1198–201 (2010).

13. Hauge, H. I. T. *et al.* Hexagonal Silicon Realized. *Nano Lett.* **15,** 5855–5860 (2015).
14. Gao, Q. *et al.* Selective-Area Epitaxy of Pure Wurtzite InP Nanowires: High Quantum Efficiency and Room-Temperature Lasing. *Nano Lett.* (2014). doi:10.1021/nl5021409
15. De Luca, M. *et al.* Polarized light absorption in wurtzite InP nanowire ensembles. *Nano Lett.* **15,** 998–1005 (2015).
16. van Dam, D. *et al.* Directional and Polarized Emission from Nanowire Arrays. *Nano Lett.* (2015). doi:10.1021/acs.nanolett.5b01135
17. Algra, R. E. *et al.* Crystal structure transfer in core/shell nanowires. *Nano Lett.* **11,** 1690–4 (2011).
18. Li, K. *et al.* Wurtzite-Phased InP Micropillars Grown on Silicon with Low Surface Recombination Velocity. *Nano Lett.* **15,** 7189–7198 (2015).
19. Standing, A. *et al.* Efficient water reduction with gallium phosphide nanowires. *Nat. Commun.* **6,** 7824 (2015).
20. Fan, S. *et al.* High Efficiency Solar-to-Hydrogen Conversion on a Monolithically Integrated InGaN/GaN/Si Adaptive Tunnel Junction Photocathode. *Nano Lett.* **15,** 2721–2726 (2015).
21. Hiraya, Y., Ishizaka, F., Tomioka, K. & Fukui, T. Crystal phase transition to green emission wurtzite AlInP by crystal structure transfer. *Appl. Phys. Express* **35502,** (2016).
22. Belabbes, A., Panse, C., Furthmüller, J. & Bechstedt, F. Electronic bands of III-V semiconductor polytypes and their alignment. *Phys. Rev. B* **86,** 75208 (2012).

23. De, a. & Pryor, C. E. Predicted band structures of III-V semiconductors in the wurtzite phase. *Phys. Rev. B* **81,** 155210 (2010).

24. Bechstedt, F. & Belabbes, A. Structure, energetics, and electronic states of III-V compound polytypes. *J. Phys. Condens. Matter* **25,** 273201 (2013).

25. Zilli, A. *et al.* Temperature Dependence of Interband Transitions in Wurtzite InP Nanowires. 4277–4287 (2015).

26. De Luca, M. *et al.* Magneto-optical properties of wurtzite-phase InP nanowires. *Nano Lett.* **14,** 4250–4256 (2014).

27. Assali, S. *et al.* Optical study of the band structure of wurtzite GaP nanowires. *J. Appl. Phys.* **44304,** 0–10 (2016).

28. Signorello, G. *et al.* Inducing a direct-to-pseudodirect bandgap transition in wurtzite GaAs nanowires with uniaxial stress. *Nat. Commun.* **5,** 3655 (2014).

29. Novák, J., Hasenöhrl, S., Vávra, I. & Kučera, M. Influence of surface strain on the MOVPE growth of InGaP epitaxial layers. *Appl. Phys. A* **87,** 511–516 (2007).

30. Gorji Ghalamestani, S., Heurlin, M., Wernersson, L.-E., Lehmann, S. & Dick, K. a. Growth of InAs/InP core–shell nanowires with various pure crystal structures. *Nanotechnology* **23,** 285601 (2012).

31. Wang, J. *et al.* Position-controlled [100] InP nanowire arrays. *Appl. Phys. Lett.* **100,** 53107 (2012).

32. Borgström, M. T. *et al.* In situ etching for total control over axial and radial nanowire growth. *Nano Res.* **3,** 264–270 (2010).

33. Borgström, M. T., Wallentin, J., Kawaguchi, K., Samuelson, L. & Deppert, K. Dynamics of extremely anisotropic etching of InP nanowires by HCl. *Chem. Phys. Lett.* **502,** 222–224 (2011).

34. Berg, A. *et al.* Growth and characterization of wurtzite GaP nanowires with control over axial and radial growth by use of HCl in-situ etching. *J. Cryst. Growth* **386,** 47–51 (2014).

35. Kim, J. Y., Kwon, M. K., Vj, L., Grego, S. & Saif Islam, M. Postgrowth in situ chlorine passivation for suppressing surface-dominant transport in silicon nanowire devices. *IEEE Trans. Nanotechnol.* **11,** 782–787 (2012).

36. Jacobsson, D. *et al.* Particle-assisted Ga(x)In(1-x)P nanowire growth for designed bandgap structures. *Nanotechnology* **23,** 245601 (2012).

37. Keplinger, M. *et al.* Core–shell nanowires: From the ensemble to single-wire characterization. *Nucl. Instruments Methods Phys. Res. Sect. B Beam Interact. with Mater. Atoms* **268,** 316–319 (2010).

38. Heiss, M. *et al.* Self-assembled quantum dots in a nanowire system for quantum photonics. *Nat. Mater.* **12,** 439–44 (2013).

39. Zhang, Y. *et al.* Polarity-driven quasi-3-fold composition symmetry of self-catalyzed III-V-V ternary core-shell nanowires. *Nano Lett.* **15,** 3128–3133 (2015).

40. Boxberg, F., Sondergaard, N. & Xu, H. Q. Elastic and piezoelectric properties of zincblende and wurtzite crystalline nanowire heterostructures. *Adv. Mater.* **24,** 4692–4706 (2012).

41. Jones, E. J., Ermez, S. & Gradečak, S. Mapping of strain fields in GaAs/GaAsP core-shell nanowires with nanometer resolution. *Nano Lett.* **15,** 7873–7879 (2015).

42. Dai, Q. *et al.* Internal quantum efficiency and nonradiative recombination coefficient of GaInN / GaN multiple quantum wells with different dislocation densities. 5–7 (2009). doi:10.1063/1.3100773

43. Jeong, H. *et al.* Carrier localization in In-rich InGaN/GaN multiple quantum wells for green light-emitting diodes. *Sci. Rep.* **5,** 9373 (2015).

44. Dhaka, V. *et al.* Protective capping and surface passivation of III-V nanowires by atomic layer deposition. *AIP Adv.* **6,** 0–7 (2016).

45. Perera, S. *et al.* Illuminating the second conduction band and spin-orbit energy in single wurtzite InP nanowires. *Nano Lett.* **13,** 5367–5372 (2013).

46. Perdew, J. P. & Wang, Y. Accurate and simple analytic representation of the electron-gas correlation energy. *Physical Review B* **45,** 13244–13249 (1992).

47. Kresse, G. & Furthmüller, J. Efficient iterative schemes for ab initio total-energy calculations using a plane-wave basis set. *Phys. Rev. B. Condens. Matter* **54,** 11169–11186 (1996).

Table 1. FEM calculated strain in the shell of WZ GaP/$In_xGa_{1-x}P$ core-shell nanowires

Indium fraction x	Average hydrostatic strain (expected in planar layer)	Strain range [min, max]
0.25	-0.7% (-2.7%)	[-0.5, -0.8]%
0.50	-1.4% (-5.1%)	[-1.0, -1.6]%
0.75	-2.0% (-7.3%)	[-1.5, -2.3]%
1	-2.6% (-9.2%)	[-2.0, -3.0]%

Captions

Fig.1 (a) Schematics of the nanowires in this work. Left: WZ GaP (blue) with the gold catalyst droplet (yellow). Right: WZ GaP/$In_xGa_{1-x}P$ core-shell nanowire ($In_xGa_{1-x}P$ in red, notice the absence of the catalyst). (b) SEM image of a representative WZ GaP/$In_xGa_{1-x}P$ core-shell sample (in this case WZ GaP/$In_{0.24}Ga_{0.76}P$). The bending due to asymmetric strain is visible in some nanowires.

Fig. 2 (a) TEM image of a WZ GaP/$In_{0.23}Ga_{0.77}P$ core-shell nanowire, showing a missing crystal plane in the 15nm thick shell (indicated by the arrow). Inset: Fast Fourier Transform of the shown image, showing the $[2\bar{1}\bar{1}0]$ zone as pattern of the wurtzite crystal structure. (b) EDS compositional line profile of the same nanowire in (a), showing the shell composition, with some limited asymmetry. Inset: HAADF image to show the executed line scan (scalebar: 100nm). The length scale of the EDX line profile has been converted to a radial profile. A slight shell thickness dishomogeneity (<10nm) is also visible. (c) 2D EDS mapping (left) and HAADF-STEM image (right) of a WZ GaP/$In_{0.24}Ga_{0.76}P$ core shell nanowire in cross section (blue: Cobalt). The core facets and the 6 shell facets parallel to them belong to the $< 10\bar{1}0 >$ family. The other 6 shell facets belong to the $< 11\bar{2}0 >$ family. (d-e) Quantified EDS element maps of the same lamella for Indium (d) and Gallium (e). (f) FEM simulations for the shell in WZ GaP/$In_{0.25}Ga_{0.75}P$ (upper panel) and WZ GaP/$In_{0.75}Ga_{0.25}P$ (lower panel) core-shell nanowires.

Fig. 3 (a) Photoluminescence spectra at 10K of various WZ GaP/$In_xGa_{1-x}P$ core shell nanowires, emitting in different spectral regions. Excitation power density: 3kW/cm^2. (b) Radial plot of PL intensity as a function of signal polarization, superimposed on a

panchromatic image of an emitting WZ GaP/$In_{0.63}Ga_{0.37}P$ nanowire. The perpendicular polarization confirms WZ emission. (c) Time-resolved photoluminescence measurements of two nanowires with different composition, showing an order of magnitude of difference in lifetime. Excitation power density: 0.2kW/cm^2. (d) Photoluminescence lifetime as a function of Indium fraction: for x≤0.28±0.04, the emission shows a lifetime well above 1ns, while for x≥0.45±0.04 the lifetime is one order of magnitude shorter. Excitation power density: 0.1 kW/cm^2. All measurements are performed at 10K on single wires transferred on SiO_2.

Fig. 4 (a) Integrated PL intensity as a function of the inverse of temperature for WZ GaP/$In_{0.24}Ga_{0.76}P$ and WZ GaP/$In_{0.63}Ga_{0.37}P$ core-shell nanowires. In WZ $In_{0.63}Ga_{0.37}P$ the increase of the integrated PL intensity above 58K, corresponding to a thermal energy of 4meV, is attributed to carrier detrapping from defects such as impurities and dislocations. Inset: comparison of the spectra at 300K, showing much stronger emission by the WZ GaP/$In_{0.63}Ga_{0.37}P$ nanowire. (b) I_{300K}/I_{10K} ratio as a function of Indium fraction x. All samples with x≤0.28±0.05 showed a ratio around 10^{-4}, while for x≥0.41±0.04 the ratio strongly increases, up to 0.18. (c) Experimental and simulated data of the main optical transitions in WZ $In_xGa_{1-x}P$. Blue (dark red) circles: emission attributed to band to band Γ_{7C}-Γ_{9V} (Γ_{8C}-Γ_{9V}-related DAP) transition. Green (bright red) triangles: data from literature for the Γ_{7C}-Γ_{9V} (Γ_{8C}-Γ_{9V}) transition. Lines: calculated energy values of the optical transitions in WZ $In_xGa_{1-x}P$. Green solid line: Γ_{7C}-Γ_{9V} transition. Red solid line: Γ_{8C}-Γ_{9V} transition. The Γ_{8C}-Γ_{7C} crossover is in this way estimated to lie at x=0.53. Green (red) dotted line: simulated Γ_{7C}-Γ_{9V} (Γ_{8C}-Γ_{9V}) transition

under average compressive hydrostatic strain. Data for average compressive strain in the shell as a function of composition are taken from Table 1.

Fig. 1

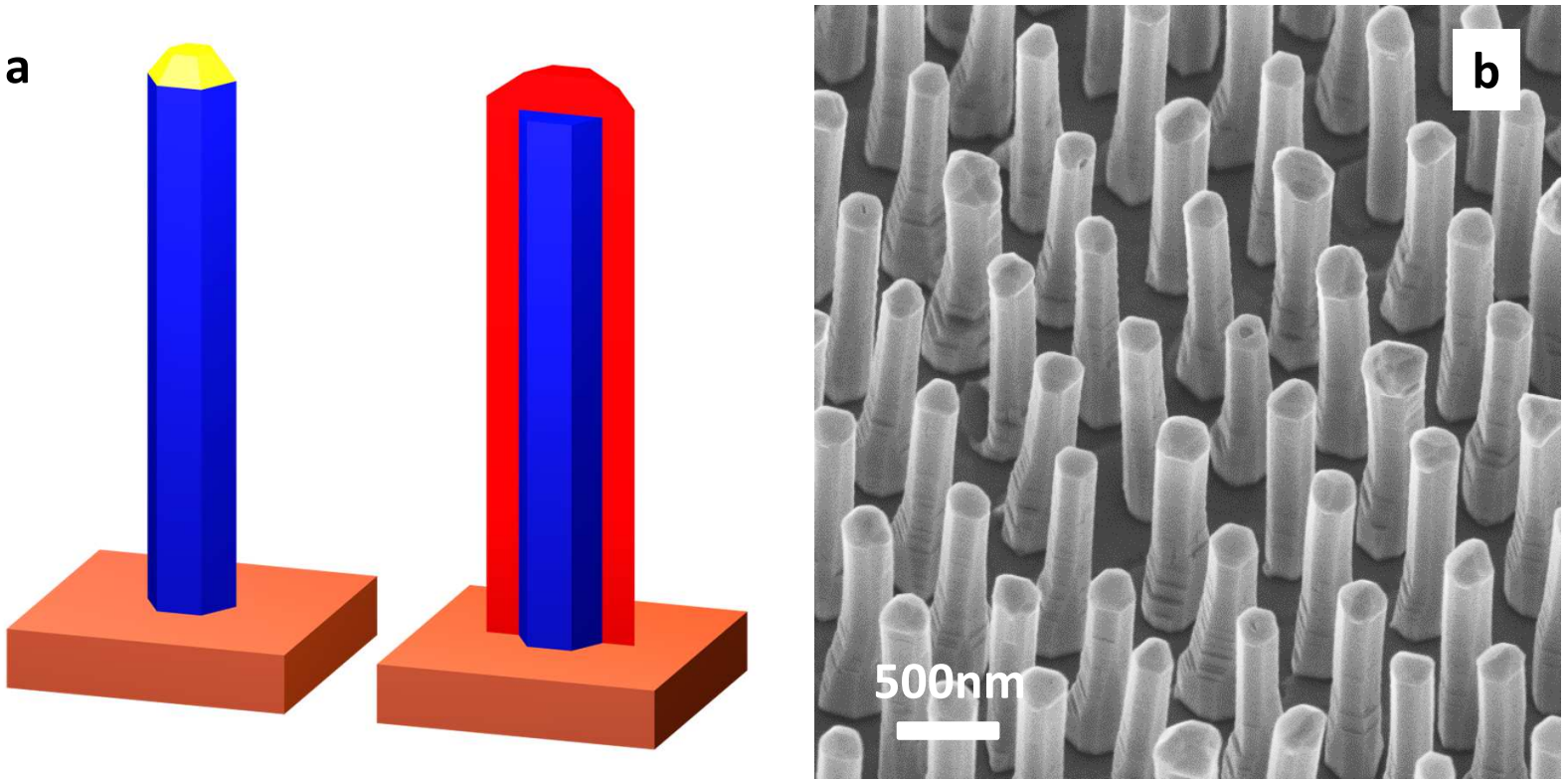

Fig. 2

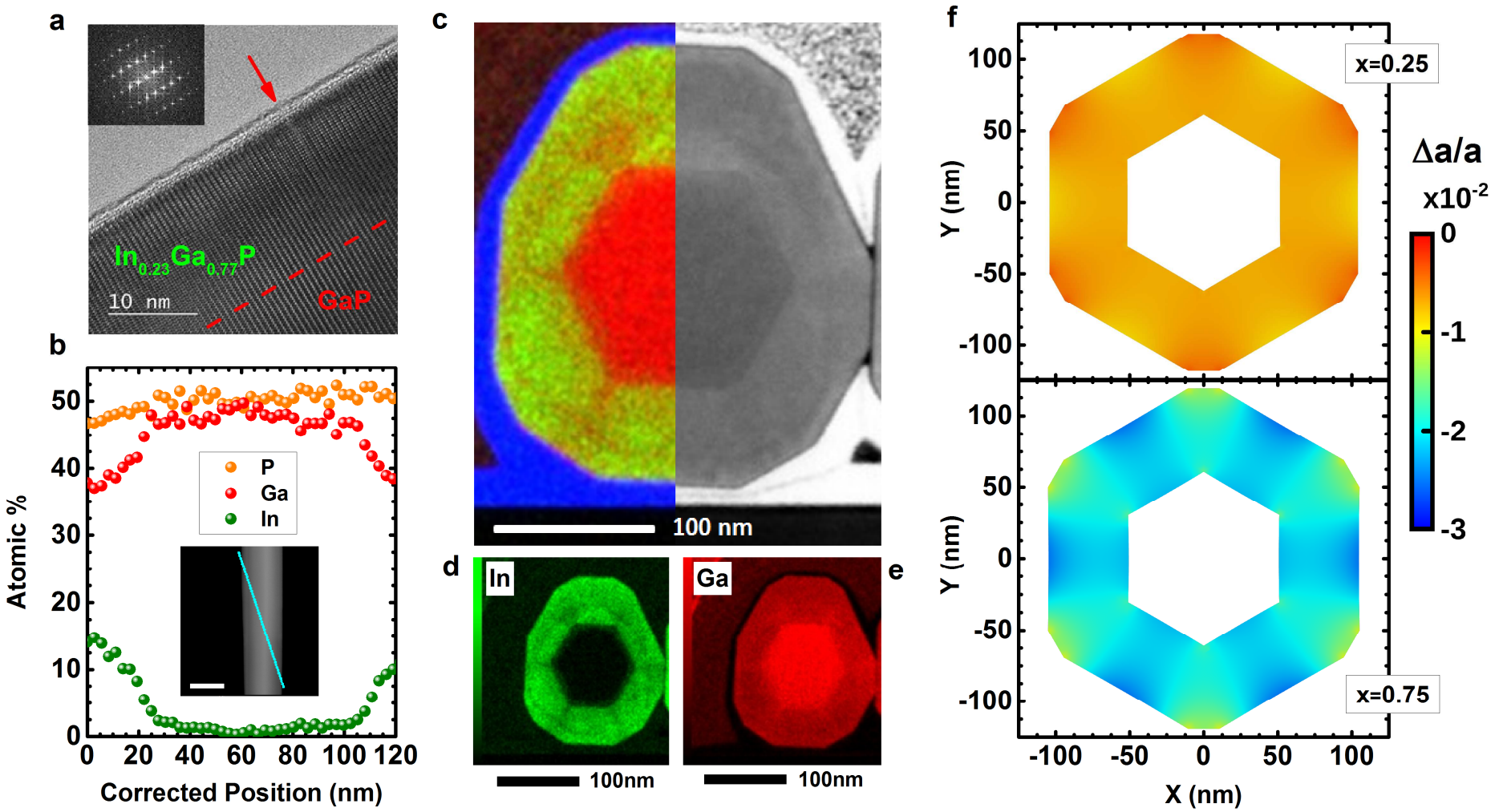
a
In0.23Ga0.77P
10 nm
GaP
b
Atomic %
Corrected Position (nm)
P
Ga
In
c
100 nm
d
In
e
Ga
100nm
100nm
f
x=0.25
x=0.75
Y (nm)
X (nm)
Δa/a
x10-2
0
-1
-2
-3

Fig. 3

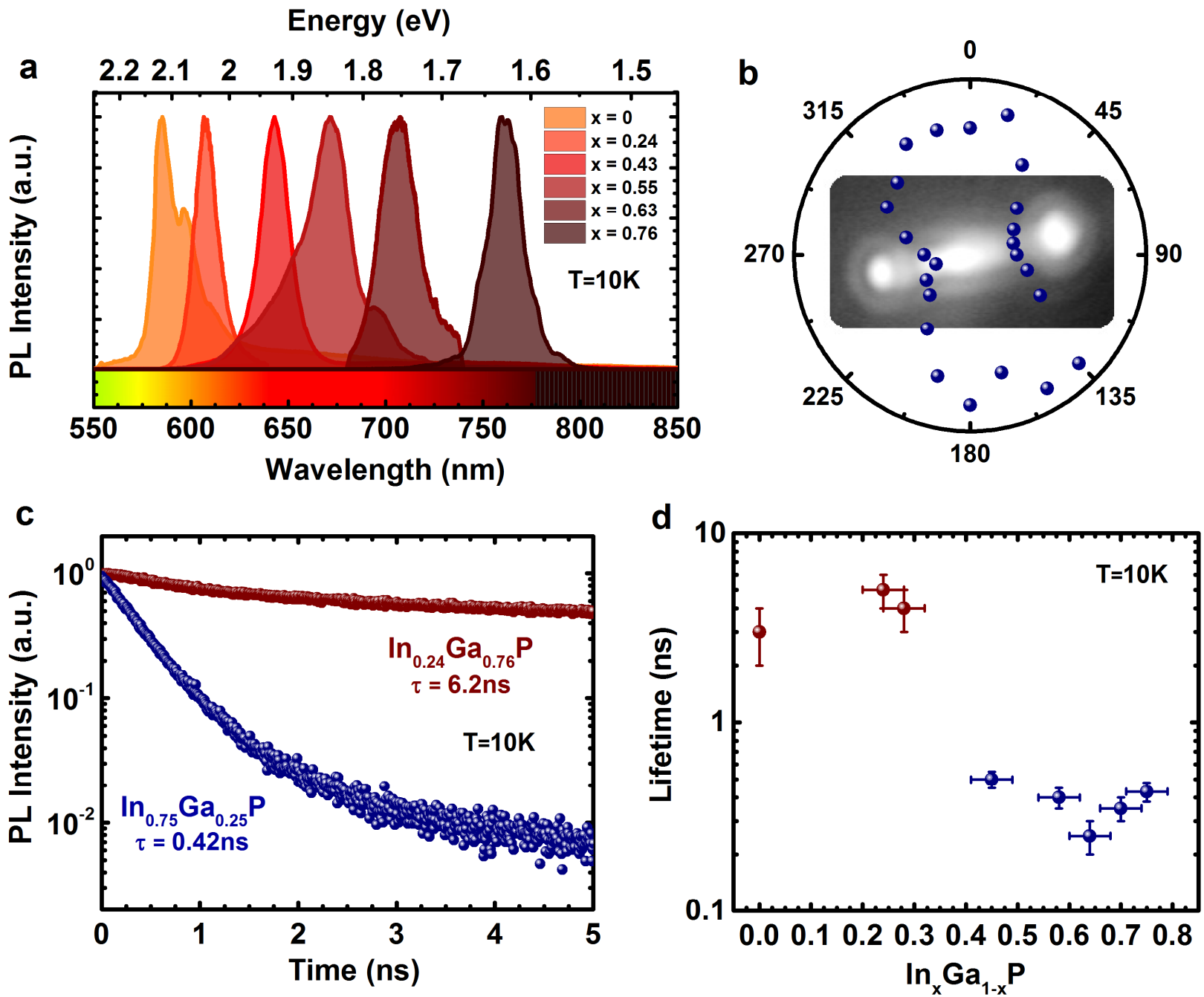
a
Energy (eV)
2.2 2.1 2 1.9 1.8 1.7 1.6 1.5
PL Intensity (a.u.)
x = 0
x = 0.24
x = 0.43
x = 0.55
x = 0.63
x = 0.76
T=10K
550 600 650 700 750 800 850
Wavelength (nm)
b
0
45
90
135
180
225
270
315
c
PL Intensity (a.u.)
10^0
10^{-1}
10^{-2}
$In_{0.24}Ga_{0.76}P$
τ = 6.2ns
T=10K
$In_{0.75}Ga_{0.25}P$
τ = 0.42ns
0 1 2 3 4 5
Time (ns)
d
Lifetime (ns)
10
1
0.1
T=10K
0.0 0.1 0.2 0.3 0.4 0.5 0.6 0.7 0.8
$In_xGa_{1-x}P$

Fig. 4

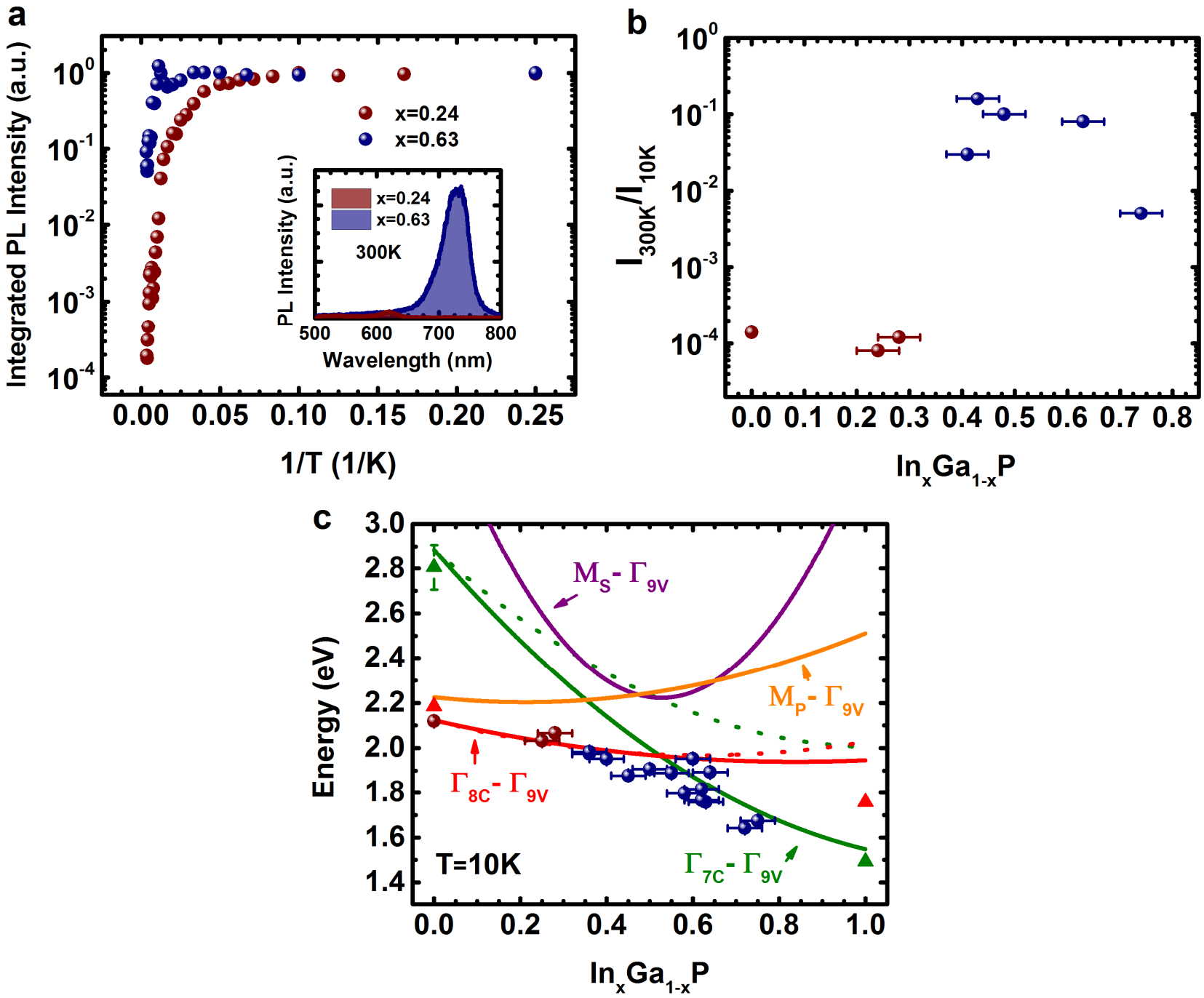
a
Integrated PL Intensity (a.u.)
1/T (1/K)
x=0.24
x=0.63
PL Intensity (a.u.)
300K
Wavelength (nm)
b
I_{300K}/I_{10K}
$In_xGa_{1-x}P$
c
Energy (eV)
M_S- Γ_{9V}
M_P- Γ_{9V}
Γ_{8C}- Γ_{9V}
Γ_{7C}- Γ_{9V}
T=10K
$In_xGa_{1-x}P$